Inward-facing glycine residues create sharp turns in β-barrel membrane proteins

Zijian Zhang[†], David Ryoo[‡], Curtis Balusek[†], Atanu Acharya[†], Marcella Orwick Rydmark[§], Dirk Linke[§], and James C. Gumbart[†*]

[†] School of Physics, Georgia Institute of Technology, Atlanta, GA 30313

[‡] Interdisciplinary Bioengineering Graduate Program, Georgia Institute of Technology, Atlanta, GA 30332

[§] Department of Biosciences, University of Oslo, Oslo, Norway

[*] To whom correspondence should be addressed; Email: gumbart@physics.gatech.edu; Phone: 404-385-0797

Abstract

The transmembrane region of outer-membrane proteins (OMPs) of Gram-negative bacteria are almost exclusively β-barrels composed of between 8 and 26 β-strands. To explore the relationship between β-barrel size and shape, we modeled and simulated engineered variants of the *Escherichia coli* protein OmpX with 8, 10, 12, 14, and 16 β-strands. We found that while smaller barrels maintained a roughly circular shape, the 16-stranded variant developed a flattened cross section. This flat cross section impeded its ability to conduct ions, in agreement with previous experimental observations. Flattening was determined to arise from the presence of inward-facing glycines at sharp turns in the β-barrel. An analysis of all simulations revealed that glycines, on average, make significantly smaller angles with residues on neighboring strands than all other amino acids, including alanine, and create sharp turns in β-barrel cross sections. This observation was generalized to 119 unique structurally resolved OMPs. We also found that the fraction of glycines in β-barrels decreases as the strand number increases, suggesting an evolutionary role for the addition or removal of glycine in OMP sequences.

Keywords : Outer membrane proteins (OMPs), Electrophysiology, β-barrels, OmpX, protein evolution

Introduction

Gram-negative bacteria have a unique cell envelope system comprising an inner membrane (IM), a peptidoglycan cell wall, and an outer membrane (OM) [1]. The OM is an asymmetric lipid bilayer composed of phospholipids in the inner leaflet and lipopolysaccharides (LPS) in the outer leaflet [2]. Nearly all outer-membrane proteins (OMPs) possess a transmembrane β-barrel. These OMPs perform various functions including nutrient transport [3, 4], antibiotic efflux [5], and biogenesis of the OM itself [6–8]. Thus, they are critically important for the survival of bacteria.

The size of OMP β-barrels ranges from 8 to 26 strands, although some multimeric barrels are even larger [9]. Unlike the structural diversity of β-barrels in general, the transmembrane region of OMP β-barrels have only one structural motif, up-and-down β-hairpins. This simple motif suggests that gene duplication has played a role in the evolution of OMP β-barrels [10–12], i.e., larger β-barrels evolve from smaller ones through the addition of one or more duplicated β-hairpin(s). Among possible evolutionary mechanisms, the probability of gene duplication is higher than mutations [11]. Given their modular structure, β-barrels can easily be expanded, at least in principle, through β-augmentation. Probing this potential growth mechanism, multiple attempts have been made to add or subtract β-hairpins to/from a β-barrel to artificially alter its pore size, although not always successfully [10, 13–16].

One common method for probing the pore size of OMPs is to measure their ionic conductance [17–22]. For example, variability in the measured conductance over time indicates a flexible channel [17] while a switch between constant low and high conductance sub-states indicates a transition between channel closing and opening [23]. OMP conductance will depend on the specific protein and species, as some OMPs are optimized for charge transport. For example, the 8-stranded OmpX from *E. coli* has six-fold higher conductance than in *Enterobacter aerogenes* [22]. Furthermore, the length and conformation of extracellular loops may also influence conductance measurements, complicating the task of determining β-barrel shapes from conductance alone. However, molecular dynamics (MD) simulations of a membrane-embedded OMP under an externally-applied electric field can provide molecular-level insights into the shape of a β-barrel as well as how it correlates with conductance.

OmpX is an 8-stranded OMP with a short extracellular loops [24, 25]. Because OmpX can be highly expressed and easily refolded in vitro [26, 27], it was previously used to build homologous β-barrel constructs with between 8 and 16 β-strands by β-hairpin duplication in experiments [10]. One might expect that increasing the number of β-strands would also increase the conductance of these

OmpX variants. However, while the conductance did increase from the 8-stranded to the 10-stranded β-barrel, increasing the barrel size to 12, 14, and 16 strands did not produce any further significant changes [10]. In fact, the 16-stranded variant has three times lower conductance than OmpF, despite the latter also possessing a 16-stranded β-barrel [28]. Why the expanded OmpX variants failed to also produce a consistent rise in conductance is unknown, although it was postulated that the cross-section of the pore was deformed from a circle, limiting their conductance [10].

In this paper, we used MD simulations and subsequent analysis to investigate the changes in shape, size, and conductance of OmpX variants with an increasing number of β-strands. We also determined how the location of specific amino acids, most notably glycine, contribute to the shape of the β-barrels of these variants as well as all other structurally resolved OMPs. These contributions are interpreted in the context of the gene duplication theory of β-barrel evolution.

Methods

Construction of OmpX variants

The WT OmpX (8-stranded) protein was taken from the NMR structure PDB ID: 2M06 [29]. Larger variants were modeled after those used in experimental electrophysiology studies in Arnold et al. [10], in which existing β-hairpins were deleted and/or duplicated to created the desired number of β-strands. The 10-stranded variant is based on OmpX64c (Arnold et al. naming [10]), the 12-stranded variant on OmpX84, the 14-stranded variant on OmpX86, and the 16-stranded variant on OmpX88. Larger β-barrels were constructed by first forcibly separating OmpX at the N-C interface, inserting the appropriate number of new β-strands, and then “healing” the new interfaces through the use of enforced hydrogen bonds via the colvars module in NAMD [30, 31]. Setup was carried out using the visualization and analysis program VMD [32].

After ensuring each constructed OmpX variant forms a stable β-barrel, they were placed in a uniform diphytanoyl phosphatidylcholine (DPhPC) membrane using CHARMM-GUI [33, 34]. DPhPC was selected to mimic the black lipid membranes used in electrophysiology experiments [10]. The systems were solvated with TIP3P water [35] and ionized with KCl to a strength of 1 M, again to match experiments. Final system sizes are from 45,000 to 50,000 atoms.

Molecular dynamics simulations

In order to avoid bias arising from the details of their construction, each β-barrel was simulated for at least 50 ns in which it was forced into a perfectly circular shape. Collective variables were designed to adjust the planar distance of every other C_α atom in the β-barrel from their collective center line until they were all equal. The resulting circular OmpX variants were then used for two subsequent equilibrium simulations using the MD program Amber [36]. Each of the two simulations was run for 3 µs with no externally imposed forces.

The end result of each of the two 3-µs equilibrium simulations was used to initialize a set of simulations with an applied electric field, mimicking the electrophysiology experiments. The field was chosen to create a potential difference (voltage) between the two sides of the system of $\pm$125 mV, $\pm$250 mV, $\pm$500 mV, $\pm$750 mV, and $\pm$1000 mV [37]. Although experimentally, the maximum voltage used was 120 mV [10], due to the limited time scales of MD simulations, a higher voltage is commonly used [38]. Simulations at $\pm$125 mV were run for 600 ns each, while those at higher voltages were run for 300 ns each. In total, 30 µs of equilibrium simulations and 36 µs of applied-field simulations were run.

All simulations used the CHARMM36 force field for lipids [39] and the CHARMM36m force field for proteins [40]. A 12-Å cut off was used for van der Waals interactions, with a force-based switching function starting at 10 Å. Long-range electrostatic interactions were calculated with the particle mesh Ewald (PME) method [41]. Temperature was maintained at 310 K using Langevin dynamics, while pressure was kept at 1 atm using a Langevin piston in NAMD and a Monte Carlo barostat in Amber. In Amber, a constant surface tension of 0 dyn/cm was enforced. The time step for initial simulations in NAMD was 2 fs. For long equilibrium and applied-field simulations in Amber, we used Hydrogen Mass Repartitioning [42, 43] and a time step of 4 fs.

Current and conductance calculations

Our approach to calculating the current and conductance follows the example of Aksimentiev and Schulten [44], using scripts provided in Comer et al. [45]. Assuming that the center of the β-barrel is at zero in the z direction and the length of the β-barrel is ℓ, we calculate the transient current I passing through the β-barrel at time $t + \Delta t/2$ by

$$I(t + \Delta t/2) = \frac{1}{\Delta t \ell} \sum_{i}^{N} q_i \left(\zeta_i(t + \Delta t) - \zeta_i(t)\right) \tag{1}$$

where

$$\zeta_i(t) = \begin{cases} z_i(t), & |z_i(t)| \leq \ell/2 \\ -\ell/2, & z_i(t) < -\ell/2 \\ \ell/2, & z_i(t) > \ell/2 \end{cases} \tag{2}$$

and q_i and z_i are the charge and z coordinate of ion i, respectively. The time step used for calculation is Δt = 0.05 ns. We found the current calculated with this time step is indistinguishable from that calculated with Δt = 0.01 ns, demonstrating that the longer time step is sufficient to capture ion motion in the OmpX variants.

In Figure 2A, every current data point is the average of the transient current I over the 300-ns simulation (600-ns for the $\pm$125 mV runs), and every conductance data point is the averaged current divided by the applied voltage. The conductance for each OmpX variant is plotted by β-strand number as the slope of the IV curve in Figure 2B. The transient conductance in SI is transient current I divided by system voltage.

Shape calculation

For each OmpX variant, an ellipse is fit to the x and y coordinates of the β-barrel C_α atoms, which are flattened onto the $z = 0$ plane, using the cv2 python library and cv2.fitEllipse function. We extract the semi-major (a) and semi-minor (b) axes from these ellipses and define the ratio of b to a as the shape of the fitted β-barrel. Thus, the shape value will fall between 0 and 1, with a perfect circle giving a shape value of 1 and a flattened ellipse giving a shape value close to zero. The pore radii over the channel coordinate of OmpX variants were measured using the program HOLE [46].

β-barrel membrane protein analysis using OPM

We downloaded all β-barrel membrane-protein structures analyzed in this paper from the Orientation of Proteins in Membranes (OPM) server [47]. To sort and filter these structures, we first searched for individual structure information using OPM's API (Application Programming Interface) and selected only those structures that included a β-strand number. Then, we further refined the list by removing any apparent duplicates. Specifically, we defined two structures as duplicates if they were the same protein from the same species but in different conformations. If the same protein had structures from two different species, they were considered two separate structures. In total, we analyzed 119 different OMP structures. Next, we identified those residues in the β-barrel of the protein by selecting protein residues between dummy atoms that mark the transmembrane region of the membrane

proteins from the OPM server. Then, we manually inspected each structure to exclude any protein residues that are inside the barrel but are not part of it. The barrel-only regions of OMPs were further processed using VMD's psfgen plugin to add hydrogens. To determine the orientation of each residue's side chain, we first imposed two different vectors on the surface area of the barrel: one from the center of the barrel to the backbone of the residue and the other from the center of the barrel to the side chain of the residue. If the backbone vector was shorter than the side-chain vector, then the residue was considered outward-facing; conversely, if the side-chain vector was shorter than the backbone vector, the residue was considered inward-facing. For glycine residues, to define the backbone and the side chain accurately, the backbone selection was changed to the HA2 atom and the side-chain selection to the HA1 atom (CHARMM force-field names). We also utilized the expectation that residues in β-strands alternate facing outward and inward to confirm the in/outward recognition results [48]. The volume and mass of amino acids were taken from Perkins [49].

Results

Shape of OmpX variants in simulations

To obtain model OmpX variants with different numbers of β-strands, one or more β-hairpins from OmpX were inserted into the 8-stranded OmpX β-barrel to match constructs used experimentally in Arnold et al. [10] (see Methods for additional details). In total, we constructed five OmpX variants with 8 (WT), 10, 12, 14, and 16 β-strands, all forced to be circular initially (Figure 1A).

OmpX variants were simulated twice in equilibrium for 3 μs each under a constant surface tension of 0. While the β-barrels of the 8, 10, 12, and 14-stranded variants deviate from their initial circular shape, remarkably, the 16-stranded variant collapses in both equilibrium simulations (Figures 1B, S1). This collapse is stabilized by the formation of a few electrostatic interactions between inward-facing residues (Figure S2), akin to the stabilizing "electrostatic core" identified in WT OmpX as necessary for folding [50]. Consequently, this variant does not contain a channel large enough for ions to pass. Also, even though the 12-stranded OmpX variant maintains a channel, it is blocked by extracellular loops that may move away over longer timescales than sampled here (Figures S3, S1).

To quantify the shape of OmpX variants, we fit the α-carbons of each β-barrel to an ellipse using the least-mean-squares method followed by calculation of the semi-minor axis length (b) and semi-major axis (a) length (Figure 1C). The ratio of b to a will have a range of $0< b/a \leq 1$, where a circle will be represented by $b/a = 1$. We define the ratio as the "shape" of a β-barrel.

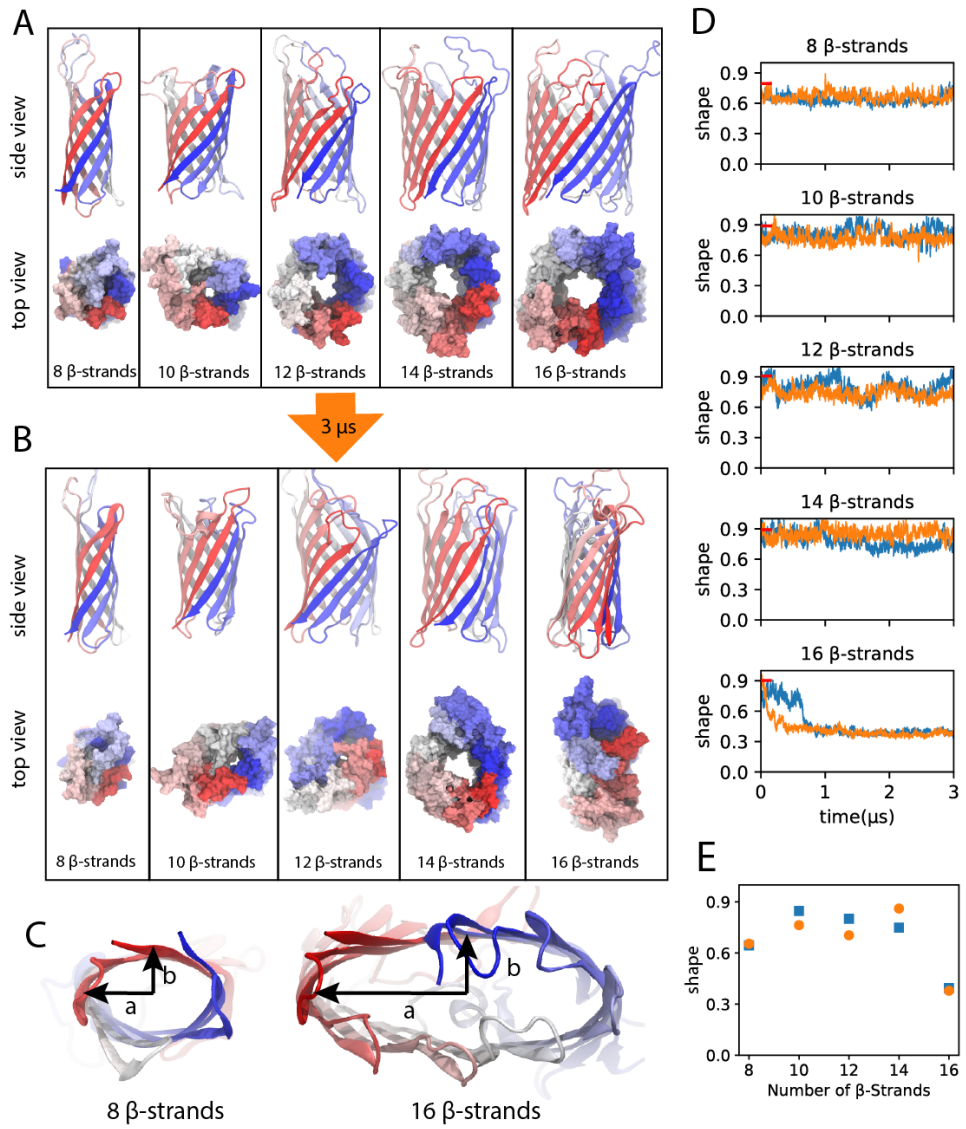

Figure 1: Equilibrium simulations of OmpX variants with different strand numbers. A. Snapshots show five OmpX variants built with different strand numbers in cartoon (side view) and surface (top view) representations colored red (N-terminus) to blue (C-terminus). **B**. Snapshots show the structure of OmpX variants after 3-μs equilibrium simulations. **C**. Representative snapshots (bottom view) of two OmpX variants at the end of 3-μs equilibrium simulations. Semi-major (a) and semi-minor (b) axes of OmpX β-barrels are shown. **D**. The shape of OmpX variants over time in the two equilibrium simulations (blue and orange, respectively). Initial shapes are marked by red dashes. **E**. Shapes of OmpX variants vs. strand numbers. The data points are calculated from the last 300-ns of each 3-μs simulation.

To investigate how the shape of OmpX β-barrels changes with an increasing number of β-strands, we tracked the shape of OmpX variants during equilibrium simulations (Figure 1D). The calculated shapes are consistent with our initial observations; the variants with 8, 10, 12 and 14 β-strands maintain a high shape value while that of the 16-stranded variant drops significantly. The shapes of OmpX variants with 10, 12 and 14 strands are about 0.8 as calculated from 3-μs equilibrium simulations (Figure 1E), suggesting that they are close to a circle. The shapes of WT OmpX (8-stranded) are relatively low with a value of about 0.6. However, the shapes of variants with 16 strands are about 0.3, demonstrating that these OmpX variants adopt a nearly flat shape. The full range of shapes for the equilibrium simulations is given for each variant in Figure S4.

Effect of β-barrel shape on conductance

After equilibrium simulations, an external electric field was applied to OmpX variants to create a voltage ranging from -1000 mV to +1000 mV. Although experimentally, applied voltages are typically limited to a few hundred millivolts, simulations routinely use larger voltages (up to 1 V) in order to improve statistics of ion permeation [38, 51]. Details of all the simulation conditions are provided in Table S1.

The currents passing through 8- and 10-stranded OmpX variants were almost uniformly zero at all applied voltages (Figure S5), apparently due to their very narrow channels (Figure 1B, S6, Table S2). Even if a single ion (Cl^- or K^+) could fit, these variants could not accommodate the accompanying solvation shells with a radius of 3.3 Å. [52] The currents for both the 12- and 16-stranded OmpX variants are almost zero under negative voltage, rising in a nonlinear fashion as voltage is increased in the positive direction (Figure 2A). In contrast, current can pass through the 14-stranded OmpX variant under negative voltage as well, although the magnitude of the current under negative voltage is much lower than under positive voltage. However, this apparent rectification may be an artifact as it is most apparent at very large applied voltages (750 - 1000 mV). Both Cl^- and K^+ ions go through the channel of OmpX, and the current contributed by K^+ is greater than that by Cl^-; the ratio of the two currents on average, K^+/Cl^-, is 1.6 (Figure S7). This ratio is similar to that observed previously in simulations of OmpF (1.2) [51] and in agreement with the experimentally measured selectivity of WT OmpX [22].

The conductance of OmpX variants was calculated from the slopes of current-voltage (I-V) plots (Figure 2B). Given the apparent non-ohmic behavior at large voltages, only data points from between -250 and 250 mV were used for these calculations. The simulated conductance values of OmpX

variants with 8 and 10 β-strands are practically zero, in contrast to the experimental values of 120 pS and 350 pS, respectively (Figures 2B, S8) [10]. However, we note that the experimental traces for the 8-stranded WT OmpX in Arnold et al. [10] were relatively noisy in comparison to larger variants, making its conductance more difficult to determine precisely. The conductance of the 12-stranded OmpX variant is approximately half of the experimental value, while that of the 14-stranded variant is close for one replica and 3× higher for the other (Figure S8). Finally, the conductance of the 16-stranded variant, is zero except for very large voltages (> 500 mV) due to the collapse of its β-barrel (Figure 1C), far below the experimental value (290 pS) [10].

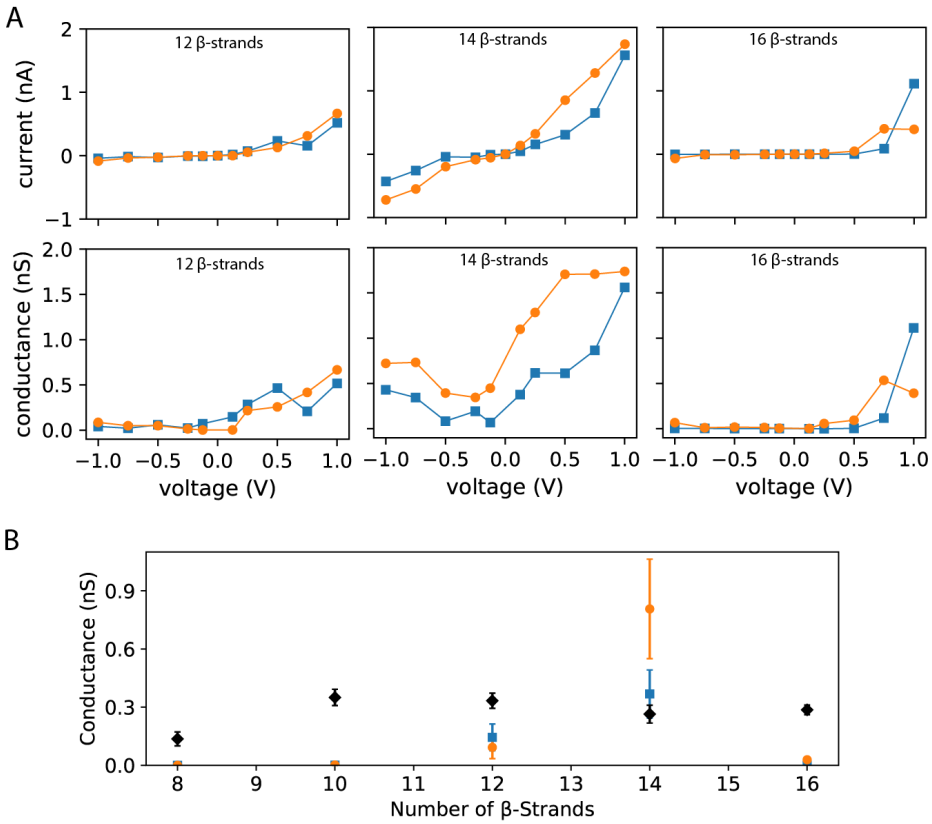

Figure 2: I-V plots and conductances of OmpX variants. **A**. Current through OmpX barrels (first row) and the corresponding conductance (second row) under voltages ranging from -1 V to +1 V for 12 (left), 14 (middle) and 16 (right) β-strands OmpX variants in two independent (blue and orange) MD simulations. **B**. Comparison between the conductance from simulations (blue and orange) and experiments (black) [10]. Simulation conductances are the slopes from a linear fit to the I-V plots.

We computed the shape for each OmpX variant under externally applied electric fields to account for any field-induced conformational changes that, in turn, impacted the conductance. We calculated the instantaneous conductance and shape for all 100 simulations performed under an electric field (Figures S9, S8). We observed that in one replica of the 16-stranded OmpX variant under voltages of

+750 mV and +1000 mV (labeled 16strands-p750-r2 and 16strands-p1000-r1, respectively, in Figure S9), the initial shape value ($\sim$0.35 as obtained from the equilibrium simulations) increases to 0.5. Therefore, the β-barrel cross-section becomes more circular under large applied positive voltage (Figure S9). Note that the 16-stranded β-barrel does not possess a channel at the end of equilibrium simulations. However, the significant change in shape under an applied electric field caused the channel to open, giving a small non-zero conductance. We speculate that over longer time scales than simulated here, a smaller applied field in line with those used experimentally could also generate the same conformational changes.

In order to quantify the relationship between the conductance and β-barrel shape, if any, we calculated the Pearson correlation coefficient between instantaneous conductance and shape from each simulation (Figure S10). A positive coefficient indicates that the conductance increases with increasing shape, while a negative coefficient indicates that the conductance decreases with increasing shape. If the coefficient is close to zero, it indicates the absence of correlation between conductance and shape. We observed that in simulations with a small OmpX variant and/or a small applied field, there is no current passing through the β-barrel (Figure S8). Additionally, the shapes of many β-barrels do not change during 300-ns applied-field simulations (600 ns for $\pm$125 mV). Thus, many coefficients fluctuate around zero. However, we found that for large positive fields, where the current was non-negligible, the coefficients are larger than +0.5 and some nearly +0.9. These large coefficients indicate a positive correlation between conductance and shape, i.e., a more circular shape (higher shape number) is positively correlated with a larger conductance.

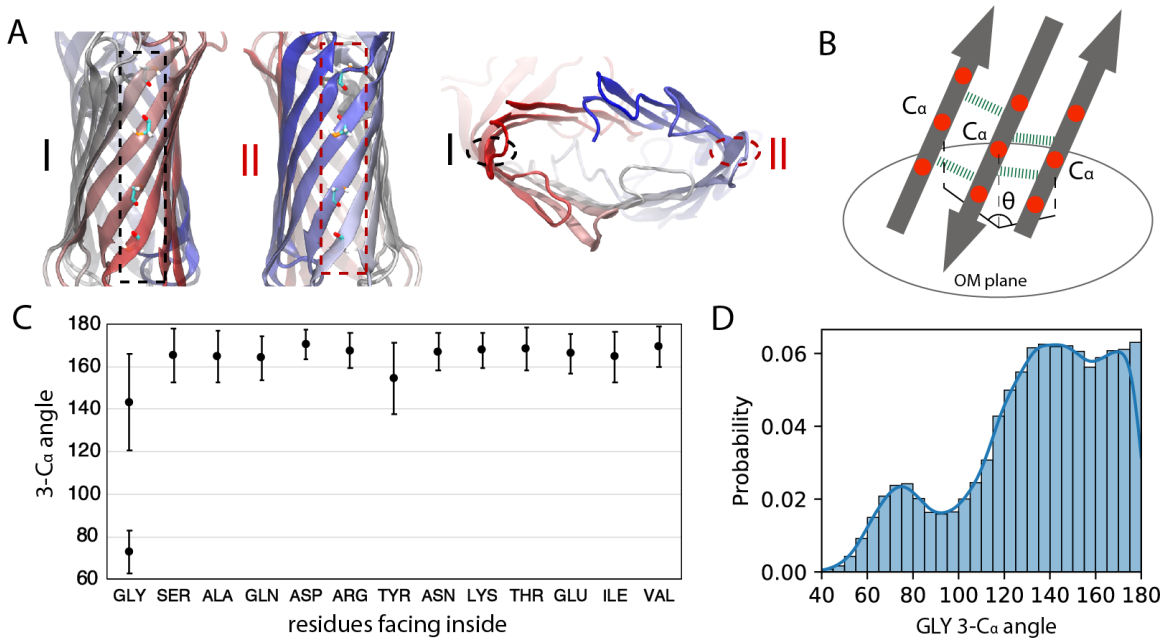

Figure 3: Location of specific amino acids plays a role in determining the overall shape of OmpX β-barrels. **A**. Side and bottom views of the 16-stranded OmpX variant β-barrels. Two sets of glycines parallel to the membrane normal, labeled I and II, are shown in licorice in the side view and marked with circles in the bottom view. **B**. Schematic definition of the 3-C_α angle. C_α atoms are identified as nearby by virtue of the adjacent backbone hydrogen bonds (green dashed lines) between their β-strands. The 3-C_α angle (θ) was then defined as the membrane-plane projection of the angle between three nearby C_α atoms and was assigned to the central amino acid. All 3-C_α angles are calculated from the inward-facing residues. **C**. Averaged 3-C_α angles of all amino acids calculated from MD simulations of OmpX variants. Error bars denote ± 1 standard deviation. Glycine is shown with two data points reflecting two apparent populations. **D**. The 3-C_α angle distribution of inward-facing glycines (GLY) in simulations.

Glycines create sharp turns in OmpX-variant β-barrel cross sections

Side chains of amino acids are responsible for many of their properties, such as hydrophobicity/hydrophilicity, charge, volume, and polarity, among others. Unsurprisingly, they also can influence the local shape of a β-barrel. Side chains of amino acids in β-barrels alternate pointing into or out of the barrel. We observed that glycines pointing into the β-barrel tend to appear in sharp turns (∼75°), forming a line parallel to the membrane normal, which amplifies their effect (Figures 3A, S11). From this observation, we hypothesized that an inward-facing glycine, which has the smallest side chain, creates an effective hole within a β-barrel (compared to larger side chains) that can be filled by tighter packing of side chains on neighboring β-strands, thereby altering the shape of the β-barrel cross section.

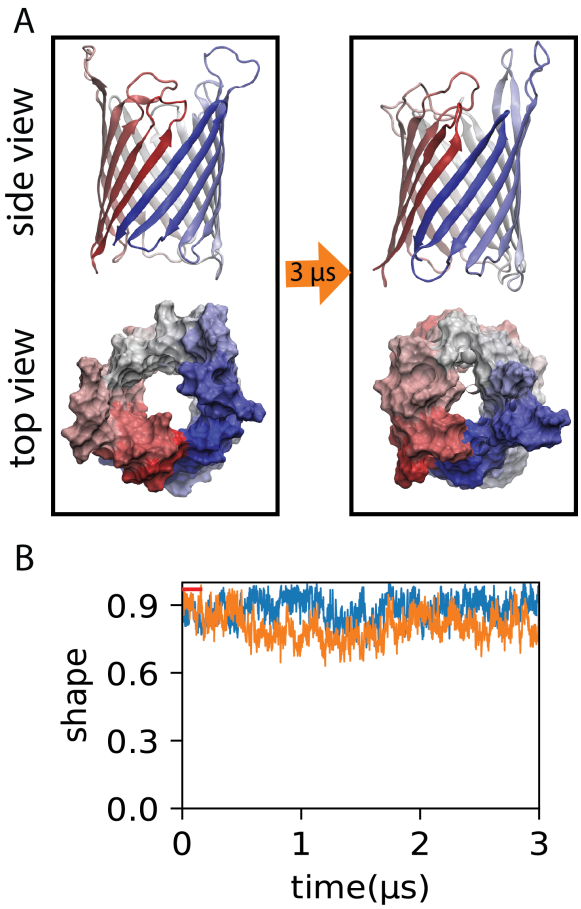

Figure 4: Equilibrium simulations of a 16-stranded OmpX variant in which inward-facing glycines have been replaced by alanine. A. Snapshots from the beginning and end of one of the simulations. **B**. The shape of OmpX variants over time in the two equilibrium simulations (blue and orange, respectively).

In order to quantify the local shape of a β-barrel near a single amino acid, we measured the angle between the C_α atoms of three amino acids from three adjacent β-strands (Figure 3B) defined

as the 3-C_α angle. All three amino acids form backbone hydrogen bonds with each other, and the value of the angle is assigned to the central amino acid. A lower value of the 3-C_α angle for an amino acid indicates a sharper turn in the barrel shape around it. Over all 30 μs of equilibrium simulations, the 3-C_α angle of inward-facing glycine stands out with an average value of 135° (Figure S12). Glycine has the lowest average 3-C_α angle and the largest standard deviation among all amino acids. We found that the low average value and the broad range of glycine 3-C_α angles originate from two separate populations (Figure 3C, D). The glycine 3-C_α angle has a large population in the range from 120° to 180° as well as a smaller population centered around 75° (Figure 3D). The smaller population around 75° represents sharp turns around glycines, while all other amino acids have larger 3-C_α angles (Figure 3C). Tyrosine possesses the second-smallest angle on average, apparently caused by its location adjacent to glycines in the OmpX variants, which only have two inward-facing tyrosines except for the 16-stranded variant with four (Figure S13). There is no apparent residue-size dependence of the 3-C_α angle except for glycine (Figure 3C), emphasizing its unique contribution to the shape of the β-barrel.

To test our claim that sharp turns are caused by glycines, we mutated 26 inward-facing glycines in the 16-stranded variant to alanine, the second-smallest amino acid. While the original 16-stranded variant quickly collapsed in simulations (Figure 3A), the mutated variant maintains its roughly circular shape over the course of both 3-μs simulations (Figure 4). The lack of collapse for the mutated variant further supports the necessity of inward-facing glycines to introduce sharp turns in the β-barrel.

Glycine-induced sharp turns are a general feature of OMPs

We hypothesized that glycine's influence on the shape of OmpX variants could be generalized to other OMPs as well. To test our hypothesis, we calculated the 3-C_α angles over all amino acids facing the inside of β-barrels from 119 structurally resolved β-barrel membrane-protein PDBs taken from the Orientation of Proteins in Membranes (OPM) server [47]. We found yet again that glycine has the lowest average 3-C_α angle of all amino acids at 146° (Figure S14). In contrast, the average 3-C_α angles for other amino acids are between 163 and 170° (Figure 5A). Serine and alanine, which are the next smallest amino acids, have the second and third lowest average 3-C_α angles in all 119 OM β-barrels. However, they are much closer to all other amino acids than they are to the glycine.

In addition to having the smallest average angle, glycine also has a much wider distribution of 3-C_α angles (70-180°) compared to other amino acids (130-180°; Figure S15, 5B). The 3-C_α angle distribution of glycine also has a small but distinct peak around 75° (Figure 5A, B), similar to that

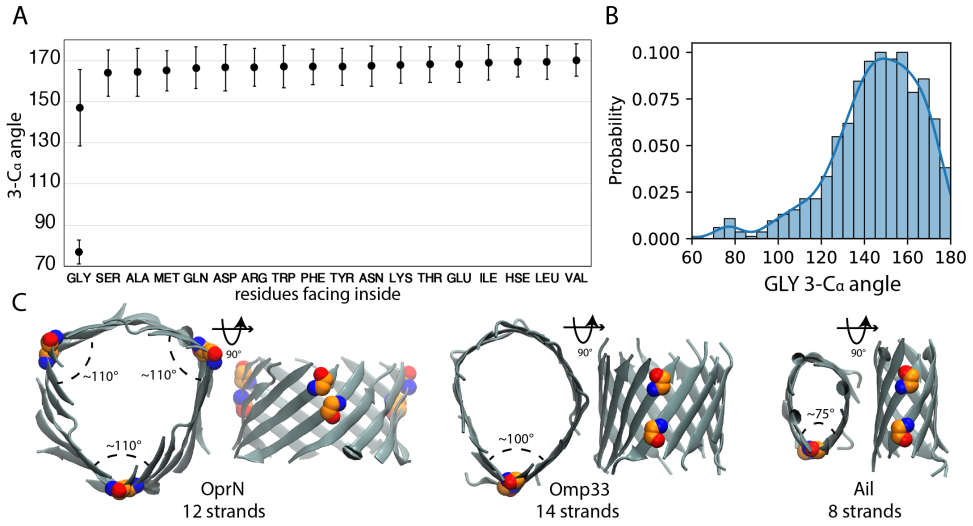

Figure 5: 3-C_α angles for inward-facing residues. A. Average 3-C_α angles of different amino acids facing inside from 119 β-barrel membrane-protein PDBs. Error bars denote ± 1 standard deviation. Glycine is shown with two data points reflecting two apparent populations. **B**. The distribution of 3-C_α angles for inward-facing glycines. **C**. Top and side view of β-barrels of OprN (PDB ID: 5AZP), Omp33 (PDB ID: 6GIE), and Ail (PDB ID: 3QRA). Glycines at the sharp turns are highlighted.

identified in OmpX variant simulations. Alanine has the second-smallest side chain after glycine, but the distribution of its 3-C_α angle is similar to those of other amino acids (Figure S15). This suggests that the missing β-carbon of glycine, not just its size alone, is a major contributor to the sharp turns. Thus, it appears that glycine is the only amino acid that has the potential to induce sharp turns in β-barrels.

To illustrate the connection between the shape of β-barrels and the location of glycines in proteins, three examples with different strand numbers and from different species of bacteria, OprN from *Pseudomonas aeruginosa* (PDB ID: 5AZP) [53], Omp33 from *Acinetobacter baumannii* (PDB ID: 6GIE) [54], and Ail from *Yersinia pestis* (PDB ID: 3QRA) [55], are shown in Figure 5C. We found that the glycines are again lined up parallel to the membrane normal at the sharp turns of the β-barrels. However, BamA from *Haemophilus ducreyi* [56] and *E. coli* [57], for example, demonstrate that glycines appear at smooth location as well (Figure S16), which contribute to the large fraction of angles greater than 140° in the distribution in Figure 5B.

We also measured the 3-C_α angles for amino acids facing outside of the barrels based on 119 β-barrel membrane-protein PDBs (Figure 6A). The average angle of glycine facing outside is around 165° and does not stand out from the average angles of other amino acids. That glycines facing outside do not alter the structure of β-barrels compared to other amino acids suggests that the sharp

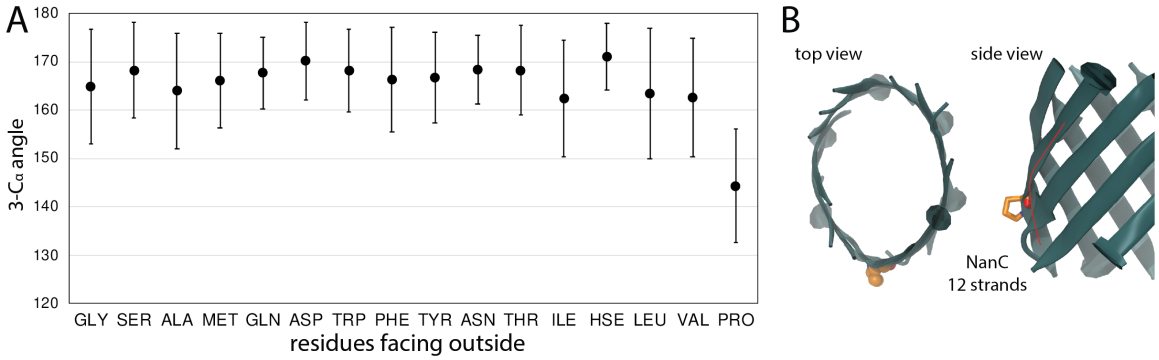

Figure 6: 3-C_α angles for outside-facing residues. A. Average 3-C_α angles of different amino acids facing outside from 119 β-barrel membrane-protein PDBs. Error bars denote ± 1 standard deviation. **B**. Top and side views of the β-barrel of NanC (PDB ID: 2WJR). A proline at a sharp turn is highlighted.

turns from those facing inward arises due to packing defects caused by the lack of β-carbons. Conversely, prolines facing outside do stand out with an average angle of $\sim$145°, which is 20° less than other amino acids. Because of their highly constrained backbone angle, prolines force bends in the β-strands and also sometimes create sharp turns in the barrel cross section. An example, NanC from *E. coli* (PDB ID: 2WJR) [58], is shown in Figure 6B.

Discussion

Outer membrane proteins (OMPs) almost exclusively have a β-barrel fold appearing in their transmembrane domains and serve a number of essential functions for the cell [9, 59]. The shape of an OMP β-barrel often plays an important role in their function, which for many is to allow substrates or ions to traverse the membrane [3, 4, 60, 61].

To examine the connection between shape and conductance, we built OmpX variants with 8 (WT), 10, 12, 14, and 16 β-strands, matching the constructs used in electrophysiology experiments in which additional strands were duplicated from existing ones [10]. Our simulations show that variants possessing β-barrels with 8–14 strands can maintain a circular shape (Figure 1E). In contrast, the 16-strand β-barrel developed a much flatter cross section than it had initially (Figure 1C). The potential collapse of large β-barrels may be addressed through the presence of long loops and/or turns bending into the β-barrels, supporting their shape. For example, the 19-stranded β-barrels of VDAC and Tom40 maintain their shapes through the presence of an N-terminal helix inside [61–63]. Previous studies demonstrated that the β-barrel of VDAC collapses when the N-terminal helix is deleted [61]. Therefore, we hypothesize that the β-barrel of large (16 strands or more) OMPs need “support arms”

(long loops, turns, or extra α-helices) or "fixed points" (periplasmic domains) to prevent collapse. Examples of one or both of these features can be seen in proteins as varied as BamA and OmpF (16 strands) [56, 64], BtuB (22 strands) [65], and LptD (26 strands) [66].

Interestingly, electrophysiology experiments revealed that conductance of OmpX variants with 10–16 strands was practically independent of size, in contrast to expectations (Figure 2B). We calculated the conductance of all OmpX variants from extensive simulations using an applied electric field, finding notable discrepancies from experiment. In particular, we failed to observe an ionic current in the 8, 10, and 16-stranded variants at voltages less than ±250 mV, despite 120 pS and 350 pS being measured experimentally, respectively [10, 22]. One possible reason for the discrepancy is that the β-barrel undergoes fluctuations to a more open state on a time scale longer than the 300–600 ns simulated; another is that the current derives from protons, which we cannot observe in classical MD simulations.

To quantitatively connect β-barrel strand number and shape, we developed a shape metric that measures the deviation from a perfect circle (Figure 1). We calculated the shape of β-barrels with different strand numbers (Figure S17) using 119 OMP β-barrel PDBs from the OPM server [47]. Even though 10-, 16-, and 26-stranded β-barrels possess a relatively flattened structure in comparison to other β-barrels, all native β-barrels maintain a shape value larger than 0.6. We measured the percentage of glycines from all the inward-facing residues within the barrel as a function of the number of β-strands (Figure 7). The results show that the percentage of glycines inside the barrel generally decreases as the number of strands increases, which is consistent with previous results from Kikuchi et al. [67]. This inverse relationship likely arises from the fact that smaller barrels have larger average curvatures and thus need more glycines to accommodate their sharper turns. Sequence alignment of 8-stranded OMPs indicates that glycines are highly conserved and appear inside of β-barrels as well [68], consistent with our finding that glycine has the lowest 3-C_α angle (Figure 3C). Considering that larger OMPs may evolve through gene duplication [10–12], replacing glycine with larger amino acids may be a necessary step to maintain a circular cross section and avoid flattening as we observed for the 16-stranded OmpX variant.

Based on glycine having the lowest average value and widest distribution of 3-C_α angles, we conclude that it behaves like a hinge in the β-barrels of OMPs, creating flexibility in the local barrel structure and often leading to sharp turns in the barrel cross section. In addition to OMPs, sharp turns due to glycines were also demonstrated in the de novo design of water-soluble β-barrels with a hydrophobic core [69]. Taken together, we can conclude that regardless of having a hydrophobic or hydrophilic core, in water or in a membrane environment, glycines facing inside the barrel can cause

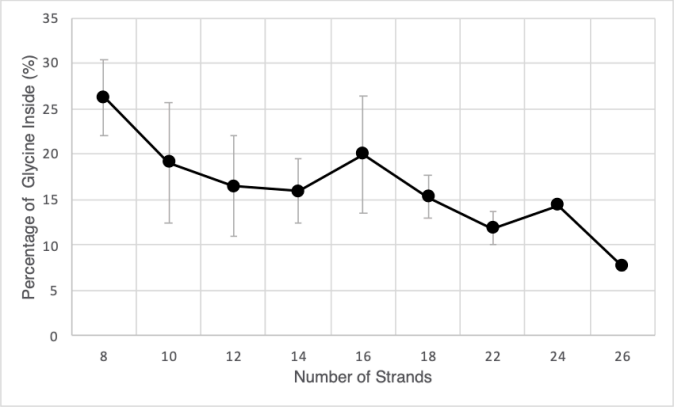

Figure 7: Percentage of glycines from the inward-facing residues as a function of the number of strands. The thin error bars at each point denote ± 1 standard deviation.

sharp turns in β-barrel structures.

In addition to the role of modulating the shape of β-barrels, the small side chain volume of glycine may affect the folding of OMPs as well. An aromatic residue in one neighboring β-strand takes advantage of the available space created by the empty side chain volume of glycine, forming a so-called "mortise-tenon" joint [70, 71]. This joint is conserved in OMPs and improve the the folding speed and stability of OMPs [71].

Considering the evolution of OMPs, the secondary structure of a region of an OMP may inter-convert between a loop and a β-strand [11]. The 3-C_α angle measurements demonstrate that glycine and proline located in β-strands can be shape-defining features of β-barrel structures. Glycines and prolines are often found in loops and turns [72], where the structure of proline is ideally suited for the β-turn and the smallest side chain of glycine provides the most flexibility. Thus, glycines and prolines in β-strands may aid their conversion to loops, reducing the size of a β-barrel. Further quantifying a possible role of these amino acids in β-barrel evolution remains an interesting avenue for future investigations.

Acknowledgments

This work was supported by the National Institutes of Health (R01-GM123169). Computational resources were provided through the Extreme Science and Engineering Discovery Environment (XSEDE; TG-MCB130173), which is supported by NSF Grant ACI-1548562. This work also used the Hive cluster, which is supported by the National Science Foundation under grant number 1828187 and is managed by the Partnership for an Advanced Computing Environment (PACE) at the Georgia Institute of Technology.

References

[1] T. J. Silhavy, D. Kahne, S. Walker, The bacterial cell envelope, Cold Spring Harb. Perspect. Biol. 2 (2010) a000414.

[2] J. C. Henderson, S. M. Zimmerman, A. A. Crofts, J. M. Boll, L. G. Kuhns, C. M. Herrera, M. S. Trent, The Power of Asymmetry: Architecture and Assembly of the Gram-Negative Outer Membrane Lipid Bilayer, Annu. Rev. Microbiol. 70 (2016) 255–278.

[3] N. Noinaj, M. Guillier, T. J. Barnard, S. K. Buchanan, TonB-dependent transporters: regulation, structure, and function, Annu. Rev. Microbiol. 64 (2010) 43–60.

[4] B. W. Lepore, M. Indic, H. Pham, E. M. Hearn, D. R. Patel, B. van den Berg, Ligand-gated diffusion across the bacterial outer membrane, Proc. Natl. Acad. Sci. U. S. A. 108 (2011) 10121–10126.

[5] J. A. Delmar, C. C. Su, E. W. Yu, Bacterial multidrug efflux transporters, Annu. Rev. Biophys. 43 (2014) 93–117.

[6] S. E. Rollauer, M. A. Sooreshjani, N. Noinaj, S. K. Buchanan, Outer membrane protein biogenesis in Gram-negative bacteria, Philos. Trans. R. Soc. Lond. B Biol. Sci. 370 (2015).

[7] S. Okuda, D. J. Sherman, T. J. Silhavy, N. Ruiz, D. Kahne, Lipopolysaccharide transport and assembly at the outer membrane: the PEZ model, Nat. Rev. Microbiol. 14 (2016) 337–345.

[8] N. Noinaj, J. C. Gumbart, S. K. Buchanan, The β-barrel assembly machinery in motion, Nat. Rev. Microbiol. 15 (2017) 197–204.

[9] J. E. Horne, D. J. Brockwell, S. E. Radford, Role of the lipid bilayer in outer membrane protein folding in Gram-negative bacteria, J. Biol. Chem. 295 (2020) 10340–10367.

[10] T. Arnold, M. Poynor, S. Nussberger, A. N. Lupas, D. Linke, Gene duplication of the eight-stranded beta-barrel OmpX produces a functional pore: a scenario for the evolution of transmembrane beta-barrels, J. Mol. Biol. 366 (2007) 1174–1184.

[11] M. W. Franklin, S. Nepomnyachyi, R. Feehan, N. Ben-Tal, R. Kolodny, J. S. Slusky, Evolutionary pathways of repeat protein topology in bacterial outer membrane proteins, Elife 7 (2018).

[12] M. Remmert, A. Biegert, D. Linke, A. N. Lupas, J. Söding, Evolution of outer membrane β-barrels from an ancestral ββ hairpin, Mol. Biol. Evol. 27 (2010) 1348–1358.

[13] M. Krewinkel, T. Dworeck, M. Fioroni, Engineering of an *E. coli* outer membrane protein FhuA with increased channel diameter, J. Nanobiotechnology 9 (2011) 33.

[14] S. Reina, A. Magrì, M. Lolicato, F. Guarino, A. Impellizzeri, E. Maier, R. Benz, M. Ceccarelli, V. De Pinto, A. Messina, Deletion of β-strands 9 and 10 converts VDAC1 voltage-dependence in an asymmetrical process, Biochim. Biophys. Acta 1827 (2013) 793–805.

[15] F. Korkmaz, K. van Pee, Ö. Yildiz, IR-spectroscopic characterization of an elongated OmpG mutant, Arch. Biochem. Biophys. 576 (2015) 73–79.

[16] J. S. Slusky, Outer membrane protein design, Curr. Opin. Struct. Biol. 45 (2017) 45–52.

[17] R. Benz, K. Bauer, Permeation of hydrophilic molecules through the outer membrane of gram-negative bacteria. Review on bacterial porins, Eur. J. Biochem. 176 (1988) 1–19.

[18] J. Nesper, A. Brosig, P. Ringler, G. J. Patel, S. A. Müller, J. H. Kleinschmidt, W. Boos, K. Diederichs, W. Welte, Omp85(Tt) from *Thermus thermophilus* HB27: an ancestral type of the Omp85 protein family, J. Bacteriol. 190 (2008) 4568–4575.

[19] A. S. Delattre, B. Clantin, N. Saint, C. Locht, V. Villeret, F. Jacob-Dubuisson, Functional importance of a conserved sequence motif in FhaC, a prototypic member of the TpsB/Omp85 superfamily, FEBS J. 277 (2010) 4755–4765.

[20] J. F. Stegmeier, C. Andersen, Characterization of pores formed by YaeT (Omp85) from *Escherichia coli*, J. Biochem. 140 (2006) 275–283.

[21] L. E. Mallarino, E. Fan, M. Odermatt, M. Müller, M. Lin, J. Liang, M. Heinzelmann, F. Fritsche, H. J. Apell, W. Welte, TtOmp85, a β-barrel assembly protein, functions by barrel augmentation, Biochemistry 54 (2015) 844–852.

[22] M. Dupont, E. Dé, R. Chollet, J. Chevalier, J. M. Pagès, *Enterobacter aerogenes* OmpX, a cation-selective channel mar- and osmo-regulated, FEBS Lett. 569 (2004) 27–30.

[23] A. C. Méli, H. Hodak, B. Clantin, C. Locht, G. Molle, F. Jacob-Dubuisson, N. Saint, Channel properties of TpsB transporter FhaC point to two functional domains with a C-terminal protein-conducting pore, J. Biol. Chem. 281 (2006) 158–166.

[24] J. Vogt, G. E. Schulz, The structure of the outer membrane protein OmpX from *Escherichia coli* reveals possible mechanisms of virulence, Structure 7 (1999) 1301–1309.

[25] C. Fernandez, C. Hilty, G. Wider, P. Güntert, K. Wüthrich, NMR structure of the integral membrane protein OmpX, J. Mol. Biol. 336 (2004) 1211–1221.

[26] A. Pautsch, J. Vogt, K. Model, C. Siebold, G. E. Schulz, Strategy for membrane protein crystallization exemplified with OmpA and OmpX, Proteins 34 (1999) 167–172.

[27] E. M. Lai, U. Nair, N. D. Phadke, J. R. Maddock, Proteomic screening and identification of differentially distributed membrane proteins in *Escherichia coli*, Mol. Microbiol. 52 (2004) 1029–1044.

[28] L. K. Buehler, S. Kusumoto, H. Zhang, J. P. Rosenbusch, Plasticity of *Escherichia coli* porin channels. Dependence of their conductance on strain and lipid environment, J. Biol. Chem. 266 (1991) 24446–24450.

[29] F. Hagn, M. Etzkorn, T. Raschle, G. Wagner, Optimized phospholipid bilayer nanodiscs facilitate high-resolution structure determination of membrane proteins, J. Am. Chem. Soc. 135 (2013) 1919–1925.

[30] J. C. Phillips, R. Braun, W. Wang, J. Gumbart, E. Tajkhorshid, E. Villa, C. Chipot, R. D. Skeel, L. Kalé, K. Schulten, Scalable molecular dynamics with NAMD, J. Comput. Chem. 26 (2005) 1781–1802.

[31] G. Fiorin, M. L. Klein, J. Hénin, Using collective variables to drive molecular dynamics simulations, Mol. Phys. 111 (2013) 3345–3362.

[32] W. Humphrey, A. Dalke, K. Schulten, VMD: Visual Molecular Dynamics, J. Mol. Graphics 14 (1996) 33–38.

[33] S. Jo, T. Kim, V. G. Iyer, W. Im, CHARMM-GUI: A web-based graphical user interface for CHARMM, J. Comput. Chem. 29 (2008) 1859–1865.

[34] E. L. Wu, X. Cheng, S. Jo, H. Rui, K. C. Song, E. M. Dávila-Contreras, Y. Qi, J. Lee, V. Monje-Galvan, R. M. Venable, J. B. Klauda, W. Im, CHARMM-GUI Membrane Builder toward realistic biological membrane simulations, J. Comput. Chem. 35 (2014) 1997–2004.

[35] W. L. Jorgensen, J. Chandrasekhar, J. D. Madura, R. W. Impey, M. L. Klein, Comparison of simple potential functions for simulating liquid water, J. Chem. Phys. 79 (1983) 926–935.

[36] D. A. Case, T. E. Cheatham III, T. Darden, H. Gohlke, R. Luo, K. M. Merz Jr., A. Onufriev, C. Simmerling, B. Wang, R. J. Woods, The Amber biomolecular simulation programs, J. Comput. Chem. 26 (2005) 1668–1688.

[37] J. Gumbart, F. Khalili-Araghi, M. Sotomayor, B. Roux, Constant electric field simulations of the membrane potential illustrated with simple systems, Biochim. Biophys. Acta Biomembr. 1818 (2012) 294–302.

[38] K. R. Pothula, C. J. Solano, U. Kleinekathöfer, Simulations of outer membrane channels and their permeability, Biochim. Biophys. Acta Biomembr. 1858 (2016) 1760–1771.

[39] J. B. Klauda, R. M. Venable, J. A. Freites, J. W. O'Connor, D. J. Tobias, C. Mondragon-Ramirez, I. Vorobyov, A. D. MacKerell Jr., R. W. Pastor, Update of the CHARMM all-atom additive force field for lipids: validation on six lipid types, J. Phys. Chem. B 114 (2010) 7830–7843.

[40] J. Huang, S. Rauscher, G. Nawrocki, T. Ran, M. Feig, B. L. de Groot, H. Grubmuller, A. D. MacKerell, CHARMM36m: an improved force field for folded and intrinsically disordered proteins, Nat. Methods 14 (2017) 71–73.

[41] T. A. Darden, D. M. York, L. G. Pedersen, Particle mesh Ewald: An N log N method for Ewald sums in large systems, J. Chem. Phys. 98 (1993) 10089–10092.

[42] C. W. Hopkins, S. Le Grand, R. C. Walker, A. E. Roitberg, Long-Time-Step Molecular Dynamics through Hydrogen Mass Repartitioning, J. Chem. Theory Comput. 11 (2015) 1864–1874.

[43] C. Balusek, H. Hwang, C. H. Lau, K. Lundquist, A. Hazel, A. Pavlova, D. L. Lynch, P. H. Reggio, Y. Wang, J. C. Gumbart, Accelerating Membrane Simulations with Hydrogen Mass Repartitioning, J. Chem. Theory Comput. 15 (2019) 4673–4686.

[44] A. Aksimentiev, K. Schulten, Imaging α-hemolysin with molecular dynamics: ionic conductance, osmotic permeability, and the electrostatic potential map, Biophys. J. 88 (2005) 3745–3761.

[45] J. R. Comer, D. B. Wells, A. Aksimentiev, Modeling nanopores for sequencing DNA, Methods Mol. Biol. 749 (2011) 317–358.

[46] O. S. Smart, J. G. Neduvelil, X. Wang, B. Wallace, M. S. Sansom, Hole: A program for the analysis of the pore dimensions of ion channel structural models, J. Mol. Graphics 14 (1996) 354 – 360.

[47] M. A. Lomize, I. D. Pogozheva, H. Joo, H. I. Mosberg, A. L. Lomize, OPM database and PPM web server: resources for positioning of proteins in membranes, Nucleic Acids Res. 40 (2012) D370–376.

[48] R. Dhar, R. Feehan, J. S. G. Slusky, Membrane Barrels Are Taller, Fatter, Inside-Out Soluble Barrels, J. Phys. Chem. B 125 (2021) 3622–3628.

[49] S. J. Perkins, Protein volumes and hydration effects. The calculations of partial specific volumes, neutron scattering matchpoints and 280-nm absorption coefficients for proteins and glycoproteins from amino acid sequences, Eur. J. Biochem. 157 (1986) 169–180.

[50] P. Rath, T. Sharpe, S. Hiller, The electrostatic core of the outer membrane protein X from *E. coli*, Biochim. Biophys. Acta Biomembr. 1862 (2020) 183031.

[51] S. Pezeshki, C. Chimerel, A. N. Bessonov, M. Winterhalter, U. Kleinekathöfer, Understanding ion conductance on a molecular level: an all-atom modeling of the bacterial porin OmpF, Biophys. J. 97 (2009) 1898–1906.

[52] J. N. Israelachvili, Intermolecular and surface forces, Academic press (2011).

[53] R. Yonehara, E. Yamashita, A. Nakagawa, Crystal structures of OprN and OprJ, outer membrane factors of multidrug tripartite efflux pumps of *Pseudomonas aeruginosa*, Proteins 84 (2016) 759–769.

[54] J. Abellón-Ruiz, M. Zahn, A. Baslé, B. van den Berg, Crystal structure of the *Acinetobacter baumannii* outer membrane protein Omp33, Acta Crystallogr. D Struct. Biol. 74 (2018) 852–860.

[55] S. Yamashita, P. Lukacik, T. J. Barnard, N. Noinaj, S. Felek, T. M. Tsang, E. S. Krukonis, B. J. Hinnebusch, S. K. Buchanan, Structural insights into Ail-mediated adhesion in *Yersinia pestis*, Structure 19 (2011) 1672–1682.

[56] N. Noinaj, A. J. Kuszak, J. C. Gumbart, P. Lukacik, H. Chang, N. C. Easley, T. Lithgow, S. K. Buchanan, Structural insight into the biogenesis of β-barrel membrane proteins, Nature 501 (2013) 385–390.

[57] Y. Gu, H. Li, H. Dong, Y. Zeng, Z. Zhang, N. G. Paterson, P. J. Stansfeld, Z. Wang, Y. Zhang, W. Wang, C. Dong, Structural basis of outer membrane protein insertion by the BAM complex, Nature 531 (2016) 64–69.

[58] C. Wirth, G. Condemine, C. Boiteux, S. Bernèche, T. Schirmer, C. M. Peneff, NanC crystal structure, a model for outer-membrane channels of the acidic sugar-specific KdgM porin family, J. Mol. Biol. 394 (2009) 718–731.

[59] J. M. Pagès, C. E. James, M. Winterhalter, The porin and the permeating antibiotic: a selective diffusion barrier in Gram-negative bacteria, Nat. Rev. Microbiol. 6 (2008) 893–903.

[60] A. Aunkham, M. Zahn, A. Kesireddy, K. R. Pothula, A. Schulte, A. Baslé, U. Kleinekathöfer, W. Suginta, B. van den Berg, Structural basis for chitin acquisition by marine Vibrio species, Nat. Commun. 9 (2018) 220.

[61] U. Zachariae, R. Schneider, R. Briones, Z. Gattin, J. P. Demers, K. Giller, E. Maier, M. Zweckstetter, C. Griesinger, S. Becker, R. Benz, B. L. de Groot, A. Lange, β-Barrel mobility underlies closure of the voltage-dependent anion channel, Structure 20 (2012) 1540–1549.

[62] Y. Araiso, A. Tsutsumi, J. Qiu, K. Imai, T. Shiota, J. Song, C. Lindau, L. S. Wenz, H. Sakaue, K. Yunoki, S. Kawano, J. Suzuki, M. Wischnewski, C. Sch§tze, H. Ariyama, T. Ando, T. Becker, T. Lithgow, N. Wiedemann, N. Pfanner, M. Kikkawa, T. Endo, Structure of the mitochondrial import gate reveals distinct preprotein paths, Nature 575 (2019) 395–401.

[63] S. R. Srivastava, R. Mahalakshmi, Evolutionary selection of a 19-stranded mitochondrial β-barrel scaffold bears structural and functional significance, J. Biol. Chem. 295 (2020) 14653–14665.

[64] E. Yamashita, M. V. Zhalnina, S. D. Zakharov, O. Sharma, W. A. Cramer, Crystal structures of the OmpF porin: function in a colicin translocon, EMBO J. 27 (2008) 2171–2180.

[65] C. Balusek, J. C. Gumbart, Role of the Native Outer-Membrane Environment on the Transporter BtuB, Biophys. J. 111 (2016) 1409–1417.

[66] I. Botos, N. Majdalani, S. J. Mayclin, J. G. McCarthy, K. Lundquist, D. Wojtowicz, T. J. Barnard, J. C. Gumbart, S. K. Buchanan, Structural and Functional Characterization of the LPS Transporter LptDE from Gram-Negative Pathogens, Structure 24 (2016) 965–976.

[67] N. Kikuchi, K. Fujiwara, M. Ikeguchi, β-Strand twisting/bending in soluble and transmembrane β-barrel structures, Proteins 86 (2018) 1231–1241.

[68] C. Baldermann, A. Lupas, J. Lubieniecki, H. Engelhardt, The regulated outer membrane protein Omp21 from *Comamonas acidovorans* is identified as a member of a new family of eight-stranded β-sheet proteins by its sequence and properties, J. Bacteriol. 180 (1998) 3741–3749.

[69] J. Dou, A. A. Vorobieva, W. Sheffler, L. A. Doyle, H. Park, M. J. Bick, B. Mao, G. W. Foight, M. Y. Lee, L. A. Gagnon, L. Carter, B. Sankaran, S. Ovchinnikov, E. Marcos, P. S. Huang, J. C. Vaughan, B. L. Stoddard, D. Baker, De novo design of a fluorescence-activating β-barrel, Nature 561 (2018) 485–491.

[70] D. L. Leyton, M. D. Johnson, R. Thapa, G. H. Huysmans, R. A. Dunstan, N. Celik, H. H. Shen, D. Loo, M. J. Belousoff, A. W. Purcell, I. R. Henderson, T. Beddoe, J. Rossjohn, L. L. Martin, R. A. Strugnell, T. Lithgow, A mortise-tenon joint in the transmembrane domain modulates autotransporter assembly into bacterial outer membranes, Nat. Commun. 5 (2014) 4239.

[71] M. Michalik, M. Orwick-Rydmark, M. Habeck, V. Alva, T. Arnold, D. Linke, An evolutionarily conserved glycine-tyrosine motif forms a folding core in outer membrane proteins, PLoS One 12 (2017) e0182016.

[72] M. W. Franklin, J. S. G. Slusky, Tight Turns of Outer Membrane Proteins: An Analysis of Sequence, Structure, and Hydrogen Bonding, J. Mol. Biol. 430 (2018) 3251–3265.